The University of Reading

# Modelling the Diurnal Variability of Sea Surface Temperatures

S. Pimentel[2], K. Haines[1] and N.K. Nichols[1]

NUMERICAL ANALYSIS REPORT 7/2007

[1]*School of Mathematics, Meteorology & Physics*
*The University of Reading*
*Whiteknights, PO Box 220*
*Reading, RG6 6AX UK*

[2]*Department of Earth Sciences*
*Simon Fraser University*
*Burnaby*
*BC V5A 1S6 Canada*

Department of Mathematics

# Modelling the Diurnal Variability of Sea Surface Temperatures

Sam Pimentel*, Keith Haines†, and Nancy K. Nichols‡

October 23, 2007

* Formally University of Reading now at Department of Earth Sciences, Simon Fraser University, Burnaby, British Columbia, V5A 1S6, Canada
sam_pimentel@sfu.ca
†Environmental Science Systems Centre, The University of Reading, UK
kh@mail.nerc-essc.ac.uk
‡Department of Mathematics, The University of Reading, UK
n.k.nichols@reading.ac.uk

**Abstract**

In this study a one-dimensional mixed layer ocean model is customised for the purpose of estimating the diurnal signal of temperature in the near surface ocean layer, generically the sea surface temperature (SST). The model is initially examined at three mooring locations. It is then demonstrated how operational forecast data sets can be utilised to estimate diurnal signals over a wide area. Daily diurnal variability maps are produced for a week long period over the Atlantic Ocean. These maps highlight the transient nature of diurnal SST signals with day to day changes in their magnitude and spatial distribution. The resulting diurnal variability maps are evaluated using a combination of infrared and microwave satellite derived SST observations taken over the day. These match-ups result in a zero mean error and 0.58 °C root mean square error and demonstrate the advantage of modelling the diurnal cycle over a persistence assumption.

# 1 Introduction

Intense diurnal warming of the surface of the ocean commonly occurs in low wind and clear sky conditions, when the wind-driven turbulence is insufficient to erode the near-surface re-stratification caused by absorption of solar radiation during the day. This buoyant highly stratified warm layer leads to an afternoon diurnal peak, after which the amplitude decays as surface cooling triggers oceanic convection and surface wind stress causes vertical shear instability, breaking down the diurnal thermocline [34]. Diurnal warming was reported by Stommel [43] in 1969 and has since been investigated by a number of authors at various locations e.g. [3], [34], [49], and [45].

Depending on how it is measured, the near surface warming in favourable conditions can be 3.5 °C [44], although an astounding diurnal variability of over 6 °C has been recorded [12]. In contrast, when an active wind-driven mixed layer is present, the diurnal amplitude of surface temperature seldom exceeds a few tenths of a degree.

Satellites now provide global synoptic measurements of SSTs which can be valuable for many purposes, but up until now these measurements have been difficult to make with an absolute accuracy. One reason is because SST retrievals by satellite (both infrared and microwave) are sensitive to a thin ocean surface layer which is strongly influenced by a diurnal warming effect. Sometimes the local time of SST observations are not taken into account at all when merging satellite data to produce observational products, e.g. Reynolds [36]. Another common approach is to flag and remove observations that are taken during the day in low wind speed conditions; this then reduces the likelihood of a bias due to diurnal warming. This is the approach taken by the UK Meteorological Office (UKMO) in producing its Ocean Sea Temperature and Ice Analysis (OSTIA) [42], where daytime observations recorded in wind speeds below $6\,\mathrm{ms}^{-1}$ are excluded. However, this is far from an ideal situation as winds speeds of less than $5\,\mathrm{ms}^{-1}$ account for nearly 40% of global hourly averaged winds [39]. Moreover weak winds are concentrated in the tropics and sub-tropics where the majority of ocean to atmosphere heat flux occurs and shifts in their patterns affect the global heat flux balance [39]. Therefore, accurate quantification of diurnal signals are required in order to make the best use of satellite derived SST observations.

Stuart-Menteth et al [45] produced monthly averaged and inter-annual diurnal warming maps derived solely from AVHRR day/night match-up observations. Their study revealed the extent of diurnal warming at mid-latitudes and the tropics and suggested the need for the diurnal cycle to be included in numerical models.

The diurnal cycle is a fundamental signal in the climate system [53], and is increasingly seen to have an impact on longer time scale variations. [2] and [41] show how the rectification of the diurnal cycle of SST onto the daily mean SST affects the magnitude of the variability of intra-seasonal SST in coupled atmosphere-ocean simulations. The diurnal variability of SST has a major impact on the time integrated air-sea heat flux calculations as explained by [34], [49], and [5]. Improved accuracy is attained in air-sea heat flux calculations if skin rather than bulk SST is used and temporal averaging of SST values are avoided or limited. Diurnal variability also has an important influence on mixed layer dynamics by enhancing the strength of mixing across the thermocline [24] and [40]. In addition [18] and [19] have shown how horizontal SST discontinuities are diminished by diurnal variability. Thus an ability to accurately and effectively simulate and measure the diurnal variability of SSTs will be of great benefit.

A strong boost to support the continuation and improvement of satellite SST measurements would come from their use in operational ocean forecast and NWP models. However the current generation of these models do not resolve the diurnal SST cycle and therefore problems are encountered when assimilating SST observations which are diurnally 'corrupted', which can result in aliasing. To address some of these issues, particularly the use in operational oceanography, this study focuses on the ability of a numerical model to provide local diurnal warming estimates based on operational ocean and NWP forecast input data.

The study will also use the classification of SSTs that takes into account the vertical temperature structure of the upper ocean as introduced by Donlon et al [7] and used by the Global Ocean Data Assimilation Experiment (GODAE) High Resolution Sea Surface Temperature Pilot Project (GHRSST-PP).

The paper proceeds as follows: A background to diurnal cycle modelling and the model setup used in this work is given in Section 2. Results from some initial experiments performed at upper ocean mooring sites are presented in Section 3. This work is then extended to the use of operational data sets in Section 4. In Section 5 diurnal variability maps in the Atlantic are produced and compared to satellite derived SST measurements. Finally conclusions are given in Section 6.

# 2 Modelling

## 2.1 Background

One-dimensional modelling of the oceanic mixed layer has been widely used in the development of turbulence and air-sea flux parameterisations. Such models are also suitable for modelling diurnal variability of SST as they can have a much greater near surface vertical resolution than can be achieved in a full ocean GCM. Mixed layer modelling can generally be categorised into two broad approaches: bulk and diffusion. Bulk models attempt to model the mixed layer in an integral sense (e.g. [22] and [34]). The governing equations of heat and momentum are integrated over the mixed layer and the balance of heat and momentum over the entire mixed layer is adjusted by the effects of momentum and buoyancy fluxes. On the other hand diffusion models directly parameterise the turbulent mixing and diffusion in the mixed layer (e.g. [25], [23], and [17]).

The first detailed modelling study of the diurnal cycle was by Price et al [34] who developed a bulk model dependent on the generation of shear instability at the base of the mixed layer. This model was also used by Shinoda to model diurnal variability in the western equatorial Pacific [41] and [40]. The bulk model by Kraus and Turner [22] was compared to the diffusion model of Kantha and Clayson [17] in a study by Horrocks et al [15]. They found the Kraus-Turner model could predict when diurnal thermoclines would form, but not their magnitude. The main limitation was the reliance on mechanical and buoyancy driven mixing, which under strong solar heating and low wind speeds becomes very low leading to surface heat build up, with no mechanism such as diffusion or conduction to draw heat downwards. The diffusion approach of Kantha-Clayson was more effective at producing downward mixing and thus predicting diurnal amplitudes. Hallsworth [14] compared the Price bulk model with a diffusion type model called the General Ocean Turbulence Model (GOTM) (see Section 2.2) at two mooring sites and also consistently found GOTM performing better at modelling the diurnal cycle of near surface temperatures.

Model experiments in the western Pacific warm pool suggest an upper layer resolution of order 1 metre is required to capture 90% of the diurnal variability [2] from the TAO data. However satellite observations resolve a much thinner layer and Horrocks

et al [15] used a grid layer of 2 cm, increasing exponentially with depth to 60 cm, when comparing model output to AATSR observations.

The penetration of solar radiation is also critical for diurnal modelling. A single spectral band parameterisation [30] is still widely used e.g. [2] and [40] despite its crude structure. Horrocks et al [15] implemented a 9 band parameterisation [31] while Hallsworth [14] experimented with several parameterisations including decomposing the full solar spectrum into 278 intervals. In recent years more attention has been given to the biological impact on solar absorption [28].

To attain the temporal resolution for diurnal modelling studies data from the TOGA COARE sites are often used, where high frequency meteorology (every 15 minutes) is available ([49], [40], and [2]) . Bernie et al [2] performed experiments using different flux frequencies and concluded that to capture 90% of the diurnal variability of SST, 3 hourly flux forcing was required. However, Horrocks et al [15] used 6 hourly surface fluxes from UKMO NWP analyses and then generated only the solar flux at higher frequency.

These previous studies have guided the modelling choices here.

### 2.2 Model Setup

For this study the GOTM model was used; originally published in 1999 it has been regularly extended since, [48]. For the purposes of this study we construct a non-uniform grid with 150 vertical levels, resolving a depth down to 150 metres. The top grid box is 0.030m thick, while the bottom box is 3.015m thick, based on the formula

$$h_i = 150 \frac{\tanh\left(\frac{i}{50}\right) - \tanh\left(\frac{i-1}{50}\right)}{\tanh(3)}, \tag{1}$$

where $h_i$ represents the thickness of the $i^{th}$ model layer. This grid distribution results in 67 model layers within the top 10m of ocean.

We have updated the air-sea flux module in GOTM, replacing the Kondo [21] air-sea flux parameterisation with the superior TOGA-COARE algorithm [11] and [10], and we have incorporated a cool-skin parameterisation [9] for use in validating against satellite data. The ocean radiant heating parameterisation of Paulson and Simpson [30] was replaced with a 9-band parameterisation [31] that covers the complete spectral range. The so-called 2-equation $k - \epsilon$ turbulent kinetic energy parameterisation is employed for the mixing, (see [47] for a detailed description of this turbulent closure scheme and the solution procedure).

## 3 Buoy Simulation Experiments

Initial experiments with the model were performed at three different mooring sites, the results of which are presented in this section.

## 3.1 Data

Surface Meteorological and ocean temperature observations are obtained from the Woods Hole Oceanographic Institution (WHOI) upper ocean mooring data archive. We use time series from three deployments: COARE [50], Arabian Sea [51], and the Subduction site [26]. Details of each time series is given in Table 1. The meteorological variables consist of the wind speed components $u$ and $v$, air temperature $T_a$, relative humidity $q_{\mathrm{rh}}$, and air pressure $p$. These measurements were made close to the standard heights of 10 metres for the wind speeds and 2 metres for the remaining variables. In addition measurements were taken of the down-welling short-wave radiation (SWR) and long-wave radiation (LWR), $I_{\downarrow}$ and $Q_B^{\downarrow}$ respectively. The ocean temperature observations, $\theta^{obs}(z)$, at various depths $z$ (within the top 150 m there are 29 observation depths in the Arabian Sea, 34 at COARE, and 12 at the Subduction site) are linearly interpolated onto the model grid and are used to initialise and validate the model simulations.

These rare observational time series with good temporal resolution are ideal for diurnal warming studies and the particular locations chosen at the tropics and higher latitude provide a sample of the meteorological conditions found in areas of the globe that experience diurnal variability of SSTs.

| Sites | Location | Duration | Frequency |
|---|---|---|---|
| Arabian Sea | 15 °N 61 °E | 17/10/94 – 17/10/95 | $\theta^{obs}(z)$ every 15 min<br>$u$, $v$, $T_a$, $q_{\mathrm{rh}}$, and $p$ every 7.5 min<br>$I_{\downarrow}$ and $Q_B^{\downarrow}$ every 15 min |
| COARE | 1 °S 156 °E | 01/11/92 – 01/03/93 | $\theta^{obs}(z)$ every 15 min<br>$u$, $v$, $T_a$, $q_{\mathrm{rh}}$, and $p$ every 7.5 min<br>$I_{\downarrow}$ and $Q_B^{\downarrow}$ every 15 min |
| Subduction | 26 °N 29 °W | 24/06/91 – 16/06/93 | $\theta^{obs}(z)$ every 15 min<br>$u$, $v$, $T_a$, $q_{\mathrm{rh}}$, and $p$ every 15 min<br>$I_{\downarrow}$ and $Q_B^{\downarrow}$ every 15 min |

Table 1: *Locations, deployment duration, and data frequency at the three mooring sites.*

## 3.2 Methodology

The model profile is initialised with the observed temperatures every 24 hours at local midnight, and forced with sensible and latent heat fluxes calculated from the surface meteorology (Table 1) using the Fairall air-sea flux algorithm [11], [10], together with down-welling SWR and LWR observations.

It is unusual to have such complete and accurate high frequency forcing data over ocean areas and as such the data from the three mooring sites is very rare. In recognition of this, further experiments were performed with the surface meteorological observations and the down-welling SWR and LWR from the buoys averaged over 6

hourly periods, the normal output format and frequency from NWP models. This allows us to assess the degradation from diurnal modelling that would be expected from using the NWP products over much wider areas.

Diurnally varying solar SWR forcing is the essential driver of the diurnal cycle. Surface insolation under clear skies, $I_{\downarrow}$, was calculated at every time step using the approach of Rosati and Miyakoda [37]. The Reed formula [35]

$$I_0 = I_{\downarrow}\left(1 - C_n n + 0.0019\beta\right)\left(1 - \alpha\right), \tag{2}$$

is then used to derive the total surface solar radiation, where $n$ is the fractional cloud cover; $c_n$, the cloud cover coefficient is set to 0.62; $\beta$ is the solar noon angle; and $\alpha$ the albedo. This formula is only used for higher cloud amounts $0.3 \leq n \leq 1$, with $I_0 = I_{\downarrow}\left(1 - \alpha\right)$ otherwise, [13]. However, the cloud values, $n$ are not directly observed at these sites, so the 6 hourly mean observed SWR values are used together with the calculated 6 hourly mean clear sky values to derive 6 hourly values of $n$.

$$n = \left(1 - \frac{I_{obs}}{I_{\downarrow}} + 0.0019\beta\right)/c_n. \tag{3}$$

This technique allows the SWR to be calculated at a much finer time resolution (at each model time step) based on a 6 hourly fixed cloud correction.

Equation 2 has been widely used in the oceanographic community and is surprisingly accurate for such a simple expression [29]. A comparative study of these methods by Dobson and Smith [6] found that the Reed formula gave the best long-term mean insolation values. Numerous studies have evaluated the precision of Equation (2) (e.g. [6], [38], and [20]) finding small, but different, regional biases and generally supporting its use for long time average insolation over the ocean. Calibration based on radiometric measurements can improve the accuracy for particular regions, e.g. Schiano [38] over the Mediterranean Sea reduces the transmission coefficient, $\tau$, from 0.7 to 0.66 based on aerosol and water vapour changes.

Following the suggestion of [38] the transmission coefficient and the cloud cover coefficient are adjusted based on the SWR observations taken at the mooring sites. To ensure over 90% of the SWR observations fall between the clear sky and full cloud limits of the Reed parameterisation, the transmission coefficient was kept at 0.7 at the Subduction site, reduced to 0.63 at the COARE site, and increased to 0.74 at the Arabian Sea. The cloud cover coefficient remained 0.62 at the Subduction and Arabian Sea sites, but was increased to 0.72 at the COARE site.

The ability of the model to replicate the sea temperature records, given the observed forcing, can be assessed in various ways. Comparisons are made between the observed and modelled ocean temperatures at various, or all, depths in the water column. Particular interest is paid to the temperature at the shallowest measurement which we will call the SST (0.45, 0.17, and 1.0 metres at COARE, Arabian Sea, and Subduction respectively) and the ability to model its variability.

The magnitude of diurnal warming is defined as the maximum SST (at the shallowest observed depth, $z_1^{\text{obs}}$) minus the minimum SST, over a 24 hour window starting at midnight

$$\Delta\theta_{z_1^{\text{obs}}} = \max_{0-24}\theta_{z_1^{\text{obs}}} - \min_{0-24}\theta_{z_1^{\text{obs}}}. \tag{4}$$

A diurnal warming signal of zero is given if the SST at the start is also the maximum/minimum over the day; this eliminates the misinterpretation of any cooling/warming trend. The near surface stratification is also calculated as the difference between the temperature at the shallowest observation point and at the 10 m depth, as follows;

$$\text{stratification} = \theta_{z_1^{\text{obs}}} - \theta_{10\text{m}}. \tag{5}$$

The mixed layer depth, MLD, is calculated as the depth at which the modelled/observed temperature is 0.1 °C below the maximum modelled/observed temperature, within the top 20 m. This is the same criterion used by Weller et al [52]. These additional parameters are used to assess the model simulation against observational profiles from the buoys.

## 3.3 Results

Results, shown in Table 2, reveal root mean square (RMS) SST temperature errors below 0.2 °C at all sites, while diurnal warming errors are larger. The largest diurnal warming errors are at the COARE site. However, the mean observed diurnal warming over the entire time series is greater at this location, 0.57 °C, compared with 0.48 °C at Arabian Sea and 0.26 °C at the Subduction site.

It should also be remembered that the SST is based on the uppermost observation at each site (i.e. from slightly different near surface depths). The errors in the MLD seem quite large considering the observed temperature profile is used to initialise each day. This could be revealing a sensitivity of the measure to non-local changes in the water column. The RMS error in the stratification varies only by 0.04 °C across the sites, and is always below 0.2 °C.

| | RMS Errors | | | |
|---|---|---|---|---|
| Site | SST (°C) | Diurnal Warming (°C) | MLD (m) | Stratification (°C) |
| COARE | 0.19 | 0.34 | 13.4 | 0.17 |
| Arabian Sea | 0.15 | 0.24 | 11.06 | 0.13 |
| Subduction | 0.13 | 0.20 | 21.79 | 0.14 |

Table 2: *Statistics from comparisons derived from observations and model simulations initialised daily at the mooring sites.*

The results of the reduced frequency forcing experiments are only slightly different, as can be seen in Table 3. An example of the modelled diurnal warming signals in this case are shown in Figure 1. This covers a six day period from the Arabian Sea time series. The diurnal cycles are of the order 1.5 °C and the observed variability is well replicated by the model. Some additional fine scale variability is seen in the observations particularly at the peak of the cycle during days 162 and 163 of the time series. This could be a result of wind fluctuations or passing clouds that have been smoothed over in the forcing data. Overall the mean modelled diurnal warming signals are 0.51 °C, 0.52 °C, and 0.36 °C at the COARE, Arabian Sea, and Subduction sites

respectively. This compares with the corresponding mean observed diurnal warming signals of 0.57 °C, 0.48 °C, and 0.26 °C. Thus the diurnal model is accurate on average to within a tenth of a degree for each time series, with the Arabian Sea site being most closely replicated. This suggests that the diurnal cycle can be effectively modelled with 6 hourly forcing data, although it is possible that there are locations where the occurrence of sharp wind bursts around midday are more prevalent, thus hampering the modelling effort. Nonetheless the standard output from operational weather forecasting centres is 6 hourly and the results in Table 3 show that modelling the diurnal cycle of SSTs over the global ocean should be a possibility. This topic is addressed in the next section.

| | RMS Errors | | | |
|---|---|---|---|---|
| Site | SST (°C) | Diurnal Warming (°C) | MLD (m) | Stratification (°C) |
| COARE | 0.19 | 0.36 | 15.94 | 0.18 |
| Arabian Sea | 0.19 | 0.30 | 12.99 | 0.17 |
| Subduction | 0.14 | 0.22 | 24.62 | 0.15 |

Table 3: *Statistics from comparisons derived from observations and model simulations forced with 6 hourly data and initialised daily at the mooring sites.*

# 4 NWP Forcing Experiments

In this section the GOTM model is set-up to use NWP forcing data on a larger spatial domain. The use of NWP data in diurnal variability modelling is far from ideal, particularly with regards to the use of 6 hourly wind stress values, as the diurnal cycle can be extremely sensitive to fine scale wind structure [46]. However the last section showed that when GOTM is forced with 6 hourly mean data at the mooring sites it can reasonably capture the observed diurnal variability. This was achieved by taking particular care to resolve the SWR at a finer resolution than 6 hours.

In addition the NWP forcing experiments are compared with satellite measurements of SST which are taken at various times of day in order to test whether the diurnal modelling can successfully capture some of the observed variability. For these satellite comparisons the uppermost model layer at a depth of 3 cm is compared with microwave data, and the skin temperature model is used to generate a product for comparison with IR satellite measurements.

## 4.1 Data

We use the European Centre for Medium-range Weather Forecasting (ECMWF) 1° global meteorological analyses/forecasts of 6 hourly integrated fluxes at 18:00, 00:00, 06:00, and 12:00 GMT, for surface solar radiation, 10 m wind speed components, 2 m air temperatures, and 2 m dew point temperatures, as well as sea level pressure. The

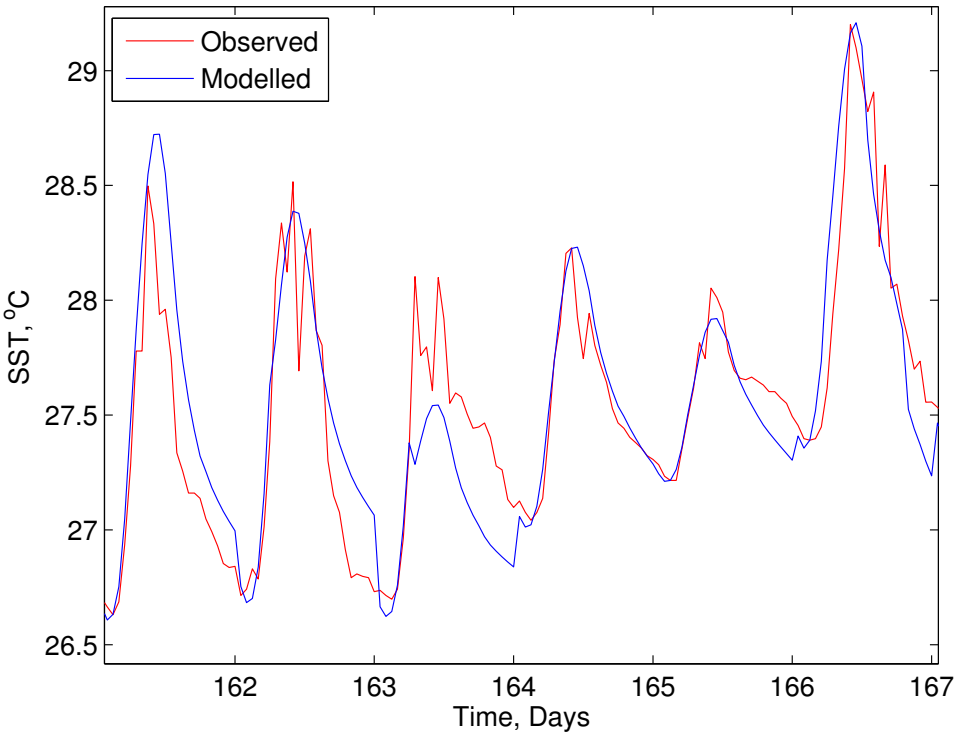


Figure 1: *Example of the modelled and observed diurnal warming signal at the Arabian Sea site.*

UKMO Forecasting Ocean Assimilation Model (FOAM) global 1° model provides analyses of ocean temperature and salinity (at depths: 5, 15, 25, 35, 48, 67, 96, and 139 metres) at 00:00 GMT.

Satellite observations include a combination of infrared (SEVIRI) and microwave (AMSR-E and TMI) SSTs from the GHRSST-PP Level-2 Pre-processed (L2P) products. The data used for this study have the GHRSST estimated bias correction applied (a correction for long-term mean biases in the sensor) and have proximity confidence values labelled 'acceptable', 'excellent', and 'diurnal'. This choice selects observations uncontaminated by cloud (for infrared) or rain (for microwave), but retains observations that potentially have a diurnal signal. The infrared retrieved SSTs are recognised as representing a skin SST and thus are compared to modelled temperatures which include a parameterised cool skin [9], whereas the microwave retrieved SSTs are representative of a temperature just below the cool skin effect and thus do not require this parameterisation.

The OSTIA product, developed at the UKMO is based on GHRSST-PP L4 combining in-situ, microwave and infra-red satellite derived SST, and is used in model initialisation. It deliberately excludes diurnal amplitudes by prohibiting daytime observations if wind speeds are below $6\,\mathrm{ms}^{-1}$. For more information on the data processing specifications adopted for GHRSST products see [8].

## 4.2 Experimental Description

As in the previous section care is again taken to convert the solar flux to a finer time resolution. ECMWF SWR is given as a 6 hourly integrated value, rather than a mean value. Integrating the Reed formula over a 6 hour window gives

$$\int_T^{T+6} I_0 dt = \int_T^{T+6} I_\downarrow \left(1 - 0.62n + 0.0019\beta\right)\left(1 - \alpha\right) dt, \tag{6}$$

where $T$ are the 6 hourly forecast times. The left hand side of Equation (6) is set equal to the ECMWF value, and Equation (6) can be rearranged to find an effective mean cloud value over this window,

$$n = \frac{\left(1 + 0.0019\beta\right)\int_T^{T+6} I_\downarrow(1-\alpha)dt - \int_T^{T+6} I_0 dt}{0.62\int_T^{T+6} I_\downarrow(1-\alpha)dt}. \tag{7}$$

If it is night, so that $\int_T^{T+6} I_\downarrow(1-\alpha)dt = 0$, then persistence $n_k = n_{k-1}$ is assumed. A check is also made to enforce the physical cloud limits $0 \leq n \leq 1$. The net surface SWR, $I_0$, used in the model run is calculated every time step using the Reed formula (2) with the 6 hourly derived cloud values.

The air-sea fluxes are calculated using the 6 hourly forecast surface meteorology (air and dew point temperature, air pressure, and $u$ and $v$ wind speeds) together with the modelled SST from GOTM, whose top layer is 3cm deep, although the air-sea flux algorithm uses the cool skin parameterisation to better represent the actual interfacial temperature at which the flux transfer takes place. This dynamic calculation allows

feedback between the modelled SST and the fluxes, and preliminary experiments found this to be better than using the prescribed fluxes from ECMWF.

The change in solar flux with depth into the ocean is parameterised as a sum of exponentials

$$f(z) = \sum_{i=1}^{n} A_i \exp\left(-K_i z\right). \tag{8}$$

In the previous section this was determined using a 9-band parameterisation [31]. Although the 9-band parameterisation covered the full spectral range, the coefficients and exponents in Equation (8) are invariant and determined from laboratory experiments using fresh water conducted in the early 1900s. The ocean, however, contains salt and suspended matter. The coefficients and exponents in the 2-band parameterisation can be modified according to Jerlov water type classification [16], an obsolete index of ocean turbidity. It has been shown that variations in solar transmission are explained almost entirely by upper ocean chlorophyll concentration in the euphotic zone, cloud amount, and solar zenith angle [28]. These factors are the basis of the Ohlmann and Siegel parameterisation [27] which is the only parameterisation to claim to resolve solar transmission variations within the top few metres of the ocean. Global remotely sensed chlorophyll maps replace the crude use of Jerlov water types. It should, however, be mentioned that variations in chlorophyll concentration are of little importance for radiant heating within the upper metre because a significant amount of the total energy exists beyond the chlorophyll sensitive wave-bands, as stated in [28]. The chlorophyll concentration values used in this work are obtained from monthly mean SeaWiFS 9 km chlorophyll-a climatologies. This data set has only been available since September 1997 and hence was not able to be utilised in the studies at the mooring sites. Tests were carried out and the Ohlmann and Siegel parameterisation together with SeaWiFS data was found to slightly improve RMS errors and reduce extremes when compared with the 9-band parameterisation.

In using a fine near surface grid the model can become very sensitive to the amount of mixing being generated in the top grid boxes, particularly in low wind speed conditions. Under low wind speed conditions the surface stress is very small and little turbulent kinetic energy (TKE) is generated. Turbulence schemes have a tendency to under produce TKE in such circumstances, but these values are of extreme importance when modelling the diurnal cycle. To prevent the extinguishing of TKE an internal wave (IW) parameterisation [17] was included to represent internal wave activity which always leaves a background residue of TKE. To enhance mixing at the surface a wave breaking parameterisation [4] was tested but was not found to improve results and was not used in the results here. Under low wind stress conditions the type of surface boundary conditions (prescribed Dirichlet conditions or a flux boundary Neumann type condition) for TKE and dissipation is important, and Neumann conditions were chosen as they were found to give the best results. Details of these tuning experiments can be found in [32].

The modelled diurnal temperatures can only be validated by comparing with individual satellite SST observations through the day. For this reason it is essential that the model starts from accurate initial temperatures, otherwise the model-observation

differences will be characteristic of any initial offset rather than differences developing through the day. The GOTM initial profiles are obtained from the UKMO operational ocean prediction system, FOAM [1], valid at 00:00 GMT each day, modified by OSTIA SSTs throughout the mixed layer to give a night time representation as close as possible to the expected conditions.

The work presented here is based in the Atlantic Ocean and therefore 00:00 GMT always represents a night time temperature (otherwise a local time correction would be needed). Details of this procedure are provided in [32].

# 5 NWP based Predictions

## 5.1 Modelled diurnal cycles

The optimised modelling arrangement incorporating IW mixing, a dynamically calculated air-sea flux, and a SeaWiFS based solar penetration, was implemented over the Atlantic Ocean ($-50\,^{\circ}$N to $50\,^{\circ}$N and $270\,^{\circ}$E to $359\,^{\circ}$E) on a $1^{\circ}$ latitude and longitude grid. Modelled diurnal variability ($\Delta\theta_{0.015\mathrm{m}}$) maps were produced for the first week of January 2006 and are shown in Figures 2 to 8. Also shown in Figures 2 – 8 for comparison are graphs of the daily mean wind stress ($\overline{\tau}$).

The pattern of the modelled diurnal warming signals shows significant variability on a day to day basis. These changes closely follow the shifting wind stress patterns, with areas of low wind stress resulting in stronger diurnal warming. This particular period is during southern hemisphere summer and several places south of the equator reach a peak SWR of $1000\,\mathrm{Wm}^{-2}$. However, these areas of high peak SWR are interspersed with areas of low peak SWR, around $500\,\mathrm{Wm}^{-2}$ due to cloud cover (as determined from the ECMWF analyses). The results suggest that the majority of the Atlantic at this time experiences low diurnal warming, between 0 and 1 °C, although some areas, predominately in the southern (summer) hemisphere, show a diurnal warming of above $1\,^{\circ}$C. There are also small areas located mainly in the latitude band $-40\,^{\circ}$ to $-20\,^{\circ}$N where the diurnal signal becomes much larger, $2-4\,^{\circ}$C. Areas of low and extremely low, $< 0.01\,\mathrm{Nm}^{-2}$, wind stress appear to be fairly good indicators of these regions of diurnal warming. The strongest diurnal warming signals only occur when very low wind stresses coincide with very strong SWR.

The area of the most significant and frequent diurnal warming is that of the latitude band $-40\,^{\circ}$N to $-20\,^{\circ}$N, the susceptibility of this region to intense diurnal warming during January has been noted before (see Figures 1 and 4 in [45]) and reveals the extent of diurnal variability in the mid latitudes, although what is particularly apparent in these maps is the intermitant nature of the warming pattern. Throughout the region a particular area can experience very strong diurnal warming one day and then the next day experience negligible diurnal warming as weather systems come and go. For example in Figure 3 centred at $(-38\,^{\circ}\mathrm{N}, 340\,^{\circ}\mathrm{E})$ is a small pocket of strong diurnal variability surrounded by a ring of strong wind stress resulting in zero diurnal warming. This system can be followed in the subsequent days as it moves east and dissipates. In the wake of the strong winds are sways of calm resulting in moderate to strong diurnal warming signals.

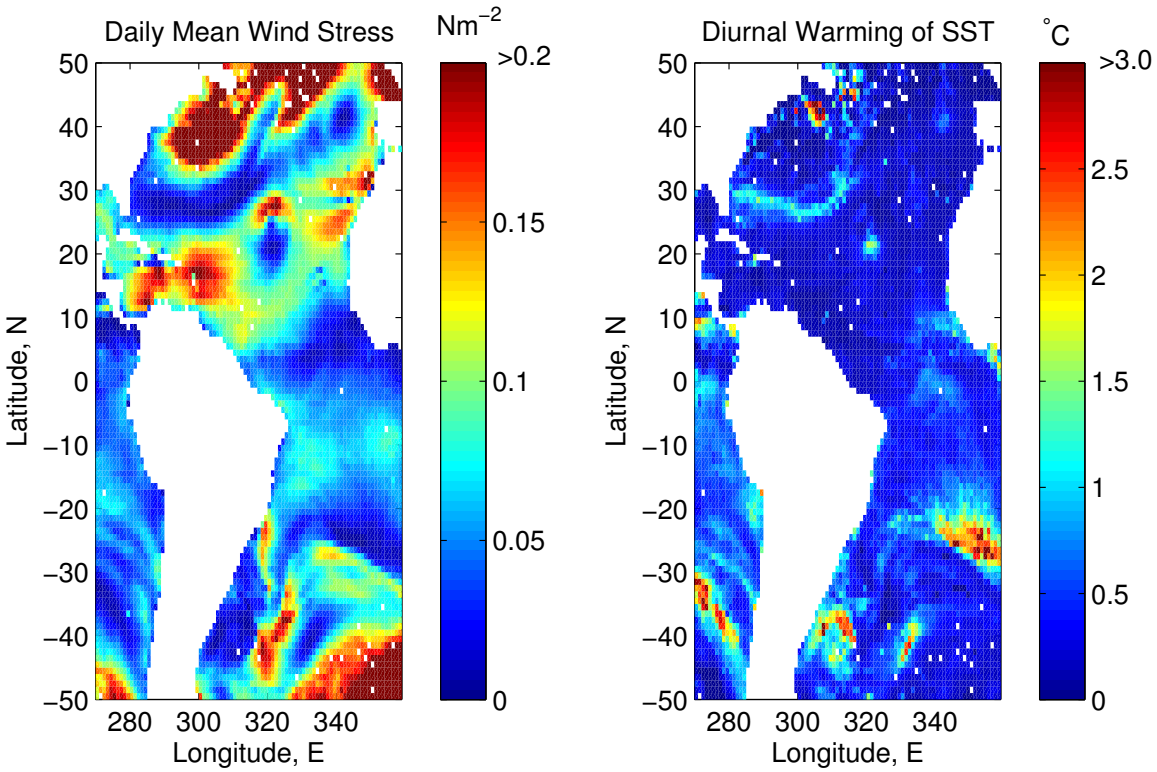


Figure 2: *A map of Atlantic Ocean showing daily mean wind stress* ($\overline{\tau}$) *and diurnal warming of SST* ($\Delta\theta_{0.015m}$) *for the* $1^{st}$ *January 2006.*

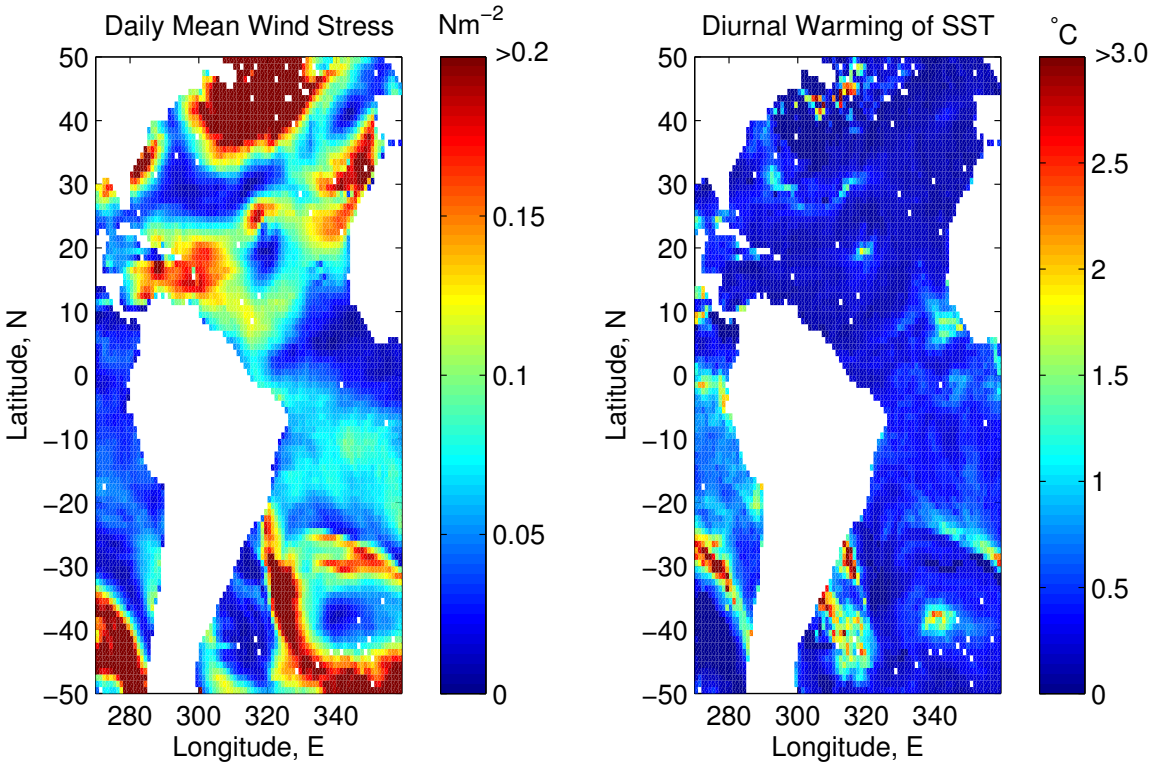


Figure 3: *A map of Atlantic Ocean showing daily mean wind stress* ($\overline{\tau}$) *and diurnal warming of SST* ($\Delta\theta_{0.015m}$) *for the* $2^{nd}$ *January 2006.*

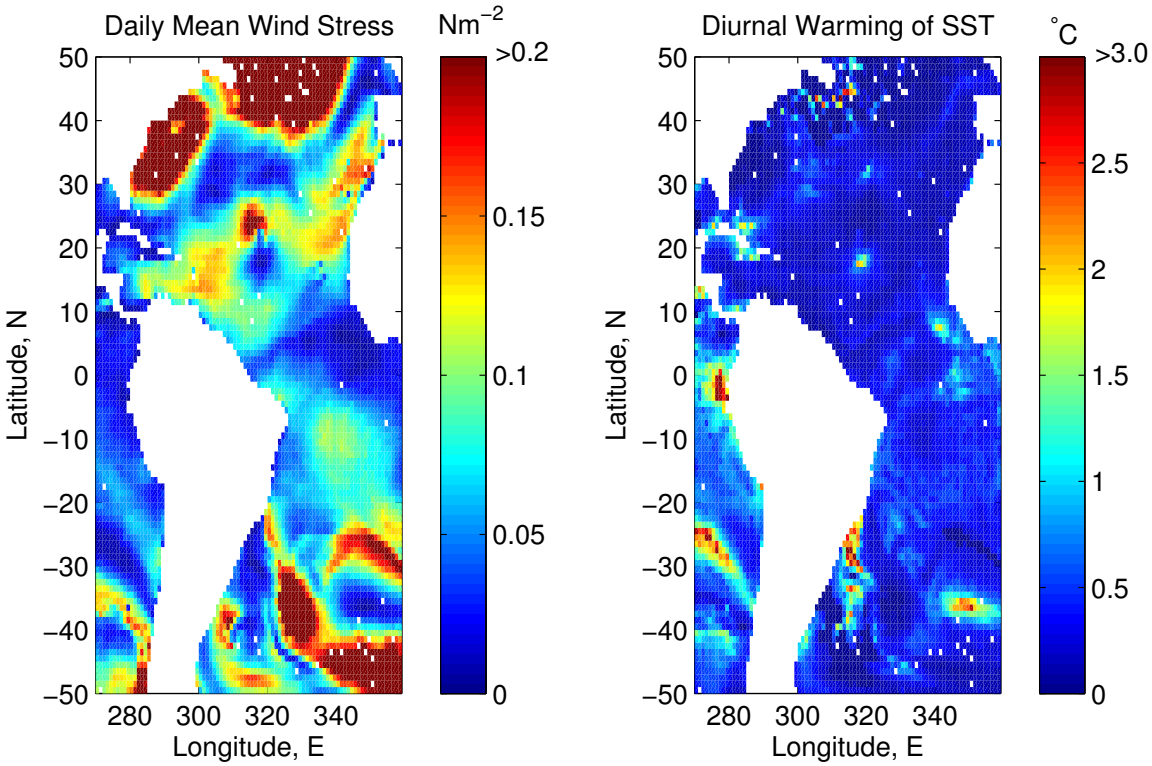


Figure 4: *A map of Atlantic Ocean showing daily mean wind stress* ($\overline{\tau}$) *and diurnal warming of SST* ($\Delta\theta_{0.015m}$) *for the* $3^{rd}$ *January 2006.*

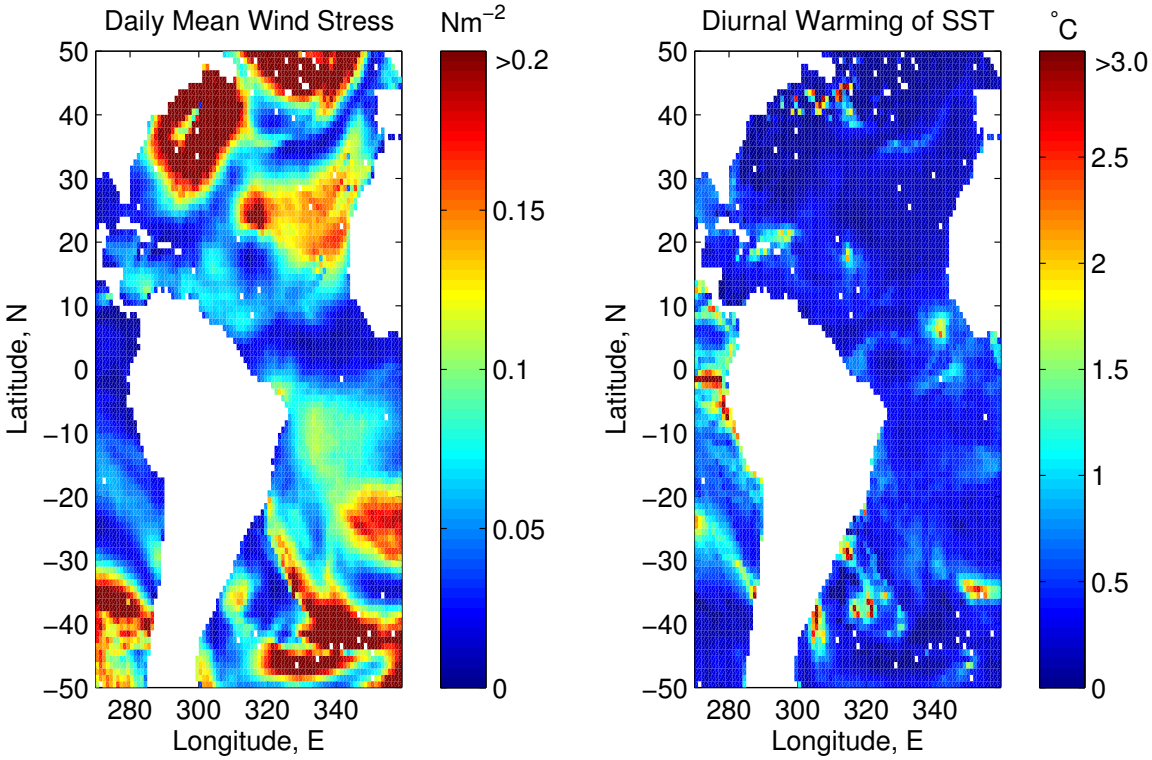


Figure 5: *A map of Atlantic Ocean showing daily mean wind stress* ($\overline{\tau}$) *and diurnal warming of SST* ($\Delta\theta_{0.015m}$) *for the* $4^{th}$ *January 2006.*

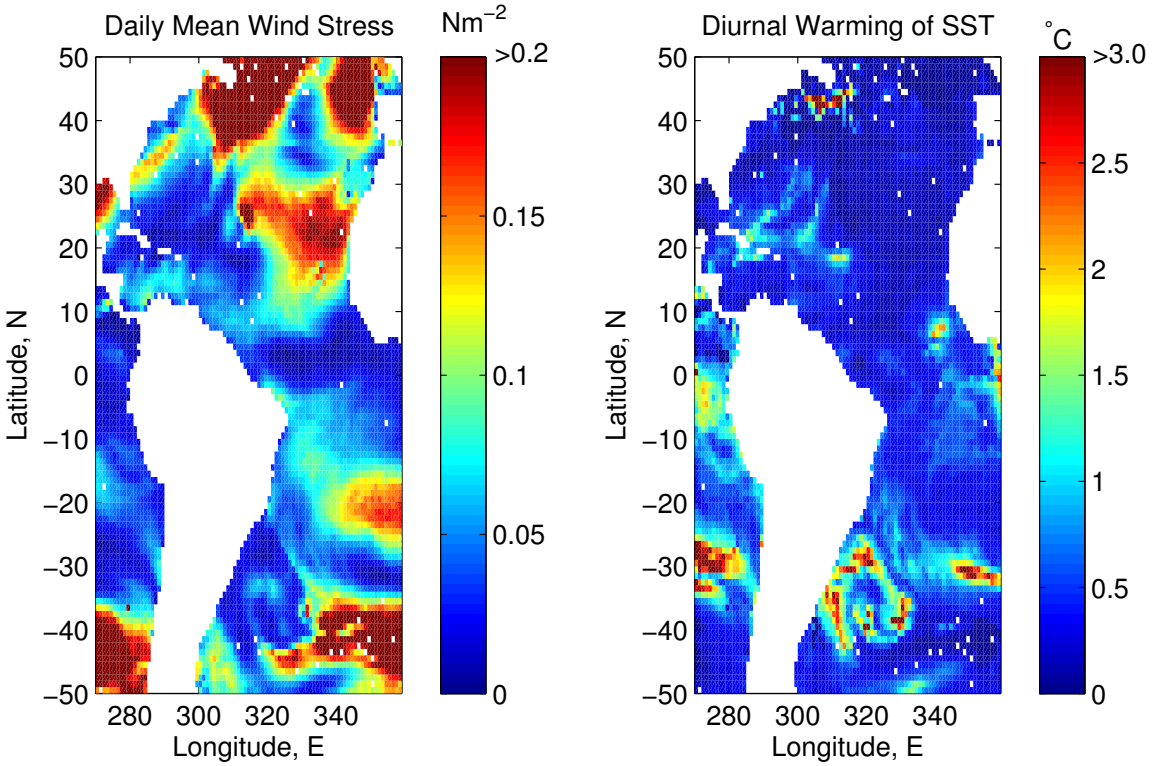


Figure 6: *A map of Atlantic Ocean showing daily mean wind stress* ($\overline{\tau}$) *and diurnal warming of SST* ($\Delta\theta_{0.015m}$) *for the* $5^{th}$ *January 2006.*

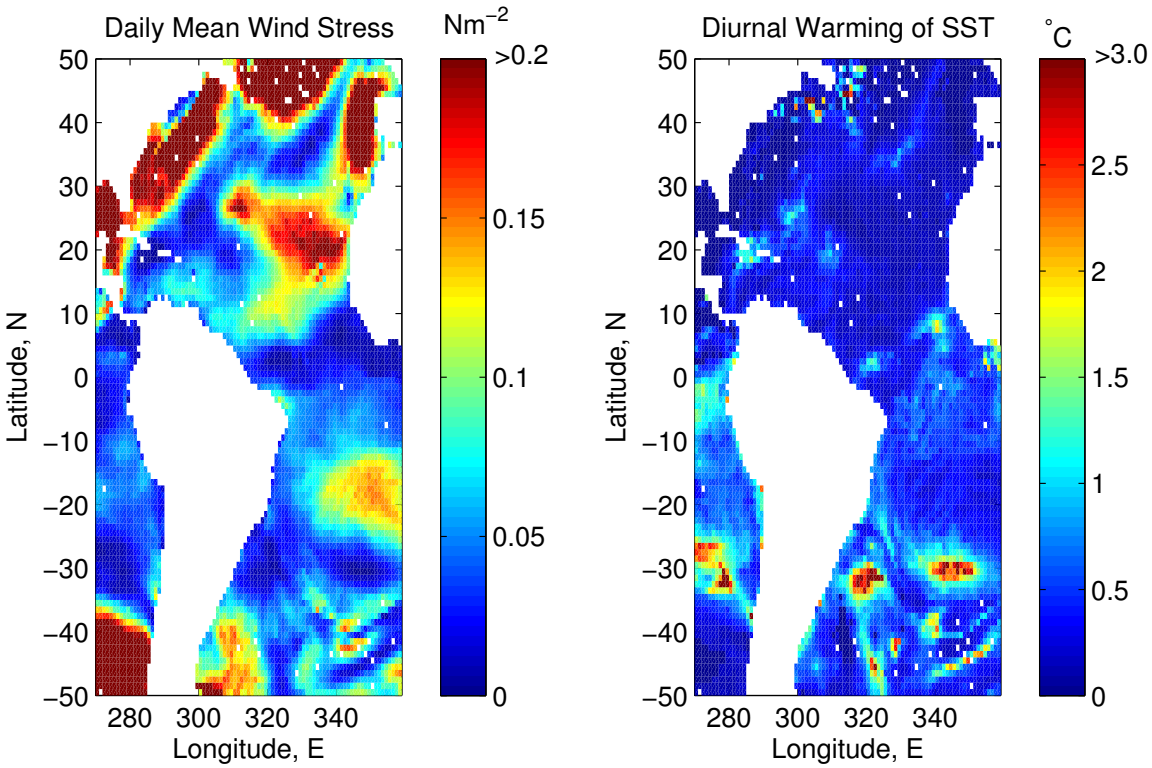


Figure 7: *A map of Atlantic Ocean showing daily mean wind stress* ($\overline{\tau}$) *and diurnal warming of SST* ($\Delta\theta_{0.015m}$) *for the* $6^{th}$ *January 2006.*

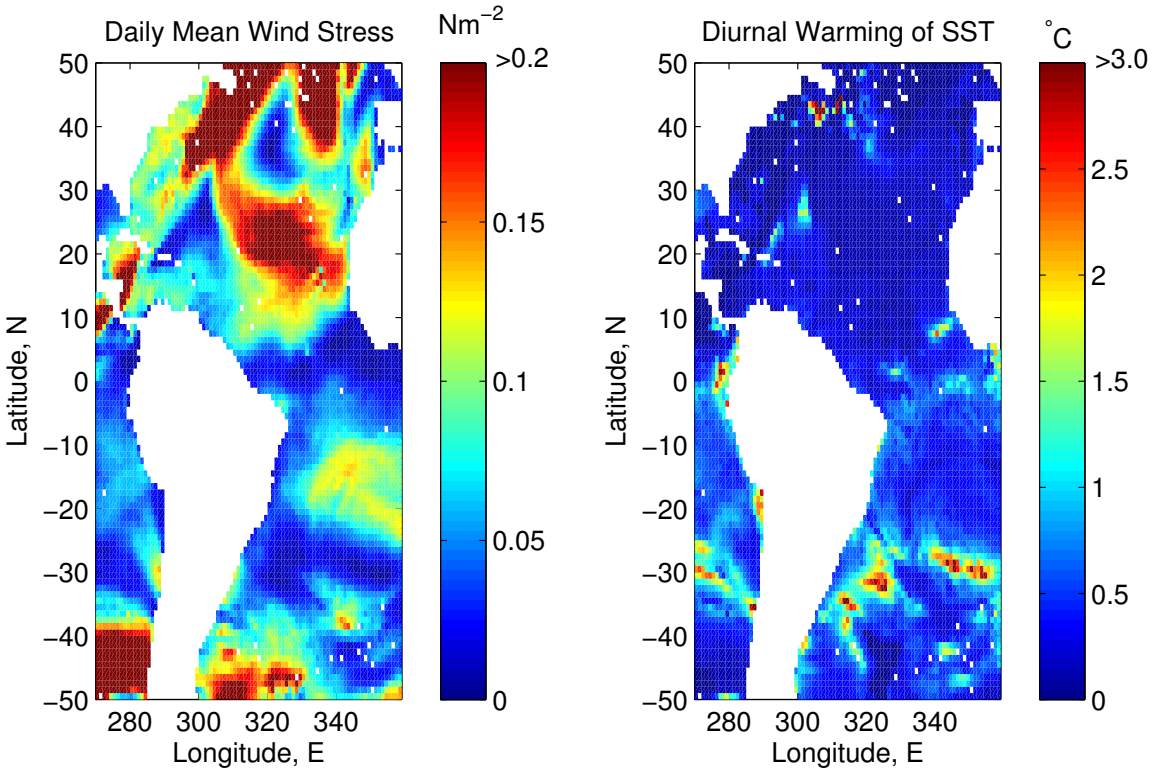


Figure 8: *A map of Atlantic Ocean showing daily mean wind stress* ($\overline{\tau}$) *and diurnal warming of SST* ($\Delta\theta_{0.015m}$) *for the* $7^{th}$ *January 2006.*

## 5.2 Satellite Validation

To assess the accuracy of the modelled diurnal warming estimates, GHRSST L2P observations from SEVIRI, AMSR-E, and TMI are compared to hourly model output. The results presented in Table 4 show that overall (last 3 rows) the model–observation differences have zero mean bias, and an RMS (error) of 0.58 °C. A slight negative bias, warmer observations than model, is seen for SEVIRI, and a slight positive bias for AMSR-E and TMI. This could represent an inherent warm bias in SEVIRI SST when compared to AMSR-E and TMI measured SST. The SEVIRI observations are measured in the infrared and are thus compared to the parameterised cool skin temperature of the model. Typical cool skin values are 0.15 °C, which although reasonable are contributing to a larger SEVIRI offset.

The table also shows that although the mean SEVIRI errors are larger than the other observation types the standard deviations (STD) are smaller as are the RMS errors. This indicates a much smaller variable component to the SEVIRI match-up errors, and that much of the error is a bias. The overall model–observation differences are shown to be the same for daytime and night time match-ups and the RMS and STD are similar, varying by only 0.02 °C. This does suggest that the use of a diurnal model is able to give as good a match to the satellite measurements during the day as during the night. Daytime here is defined as occurring between the restricted hours 10–16 (local time), and night time hours between 22–04 (local time), the model is initialised to OSTIA between the stated night time hours.

| Match-up | Number | Mean | STD | RMS |
|---|---|---|---|---|
| GOTM-SEVIRI | 28075 | −0.24 | 0.26 | 0.43 |
| Day: GOTM-SEVIRI | 7610 | −0.26 | 0.21 | 0.42 |
| Night: GOTM-SEVIRI | 6264 | −0.24 | 0.26 | 0.44 |
| GOTM-AMSRE | 26884 | 0.13 | 0.59 | 0.62 |
| Day: GOTM-AMSRE | 6009 | 0.14 | 0.51 | 0.55 |
| Night: GOTM-AMSRE | 5660 | 0.19 | 0.55 | 0.61 |
| GOTM-TMI | 22269 | 0.16 | 0.64 | 0.68 |
| Day: GOTM-TMI | 6103 | 0.15 | 0.64 | 0.67 |
| Night: GOTM-TMI | 4647 | 0.07 | 0.66 | 0.67 |
| GOTM-ALL | 77228 | 0.00 | 0.58 | 0.58 |
| Day: GOTM-ALL | 19722 | −0.01 | 0.55 | 0.55 |
| Night: GOTM-ALL | 16571 | −0.01 | 0.57 | 0.57 |

Table 4: *Comparing model output ($\theta_{skin}$ for SEVIRI and $\theta_{0.015m}$ for AMSRE and TMI) to GHRSST L2P satellite data for the Atlantic Ocean (−50 °N to 50 °N and 270 °E to 359 °E) during $1^{st} - 7^{th}$ January 2006. Results show number of match-ups, mean, standard deviation, and root mean square difference; values in* °C.

The satellite observations are also compared directly to the OSTIA combined SST product in Table 5. The satellite observations all have a negative bias (with only two exceptions), showing that the satellite observations are slightly warmer than OSTIA

on average. This should be expected as OSTIA represents a night time or foundation temperature, i.e. the minimum temperature to be expected during the day, whereas the match-ups here compare all observations, including those that contain a diurnal signal. When compared to the GOTM-observation comparisons in Table 4 we see that the negative biases are no longer widespread (with the exception of SEVIRI), i.e. GOTM is warmer than OSTIA (although the skin temperature is cooler). The GOTM model is shown to improve on the OSTIA when considering all observations and looking at the mean revealing the benefit of a modelled diurnal cycle. Comparing results from the two tables also shows that the majority of the standard deviation entries are lower when using the model as opposed to just OSTIA. However, the RMS errors are seen to be lower in general for the OSTIA only comparison.

Technically OSTIA applies a sensor specific bias correction before it ingests observations, which is designed to take account of atmospheric phenomena, such as aerosols and dust, but also, in the case of SEVIRI, skin to bulk differences. The skin effect appears to take GOTM further from the SEVIRI observations as without it GOTM on average would be closer to the SEVIRI observations than OSTIA. This suggests that the SEVIRI retrieval algorithm, which empirically is tuned against buoy measurements, has blurred the distinction between skin and bulk SSTs. This result highlights the need to understand and distinguish between varies sources of error in the observations so that maximal information content can be acquired from the satellite measurements.

| Match-up | Number | Mean | STD | RMS |
|---|---|---|---|---|
| OSTIA-SEVIRI | 28447 | −0.14 | 0.31 | 0.36 |
| Day: OSTIA-SEVIRI | 7693 | −0.14 | 0.27 | 0.33 |
| Night: OSTIA-SEVIRI | 6376 | −0.12 | 0.32 | 0.36 |
| OSTIA-AMSRE | 27364 | −0.03 | 0.55 | 0.55 |
| Day: OSTIA-AMSRE | 6068 | 0.06 | 0.48 | 0.49 |
| Night: OSTIA-AMSRE | 5803 | −0.03 | 0.60 | 0.60 |
| OSTIA-TMI | 23750 | −0.01 | 0.65 | 0.65 |
| Day: OSTIA-TMI | 6137 | 0.05 | 0.60 | 0.60 |
| Night: OSTIA-TMI | 5382 | −0.20 | 0.72 | 0.78 |
| OSTIA-ALL | 79561 | −0.06 | 0.52 | 0.53 |
| Day: OSTIA-ALL | 19898 | −0.02 | 0.48 | 0.48 |
| Night: OSTIA-ALL | 17561 | −0.11 | 0.57 | 0.59 |

Table 5: *Comparing OSTIA, used as the initial condition for the Atlantic model runs, to GHRSST L2P satellite data for the Atlantic Ocean (*$-50\,^{\circ}$N *to* $50\,^{\circ}$N *and* $270\,^{\circ}$E *to* $359\,^{\circ}$E*) during* $1^{\text{st}} - 7^{\text{th}}$ *January 2006. Results show number of match-ups, mean, standard deviation, and root mean square difference; values in* °C.

# 6 Discussion and Conclusions

Progress has been made in understanding and advancing the ability to numerically model diurnal variability at the near surface ocean. A widely used one-dimensional mixed layer model, GOTM, is optimised for the purposes of diurnal cycle modelling using state-of-the-art parameterisations for air-sea flux and ocean radiant heating. It is tuned against high frequency observations from buoy data at three different sites representing a range of ocean and meteorological conditions. It is demonstrated that accurate diurnal warming estimates can still be achieved for these buoy sites using only 6 hourly data suggesting that 6 hourly NWP data could be used in determining diurnal cycles over wide areas.

A grid of 1-D GOTM models were run over a wide area of the Atlantic ocean forced by NWP data, and the results used to produce daily spatial maps of the diurnal warming signal in SST. This mesh of models forced with NWP data is shown to be a very useful method, viz, in identifying areas of diurnal warming and quantifying diurnal signals in observational SST data. The magnitude and spatial distribution of diurnal SST signals are shown to have variability on a day to day basis. The resulting diurnal warming maps are of interest in building a climatology of the magnitude and extent of diurnal cycles in SSTs, and as such furthers our understanding of ocean-atmosphere interaction.

For a week long period over the Atlantic Ocean a comparison between a combination of IR and MW satellite derived SST observations and the modelled diurnal cycles resulted in a zero mean error and RMS and STD errors of 0.58 °C.

Plots such as Figures 2 – 8 are a first attempt to produce such maps based on model output and they provide added value in several respects. They can be produced globally on a daily basis, as they do not rely on particular overpass paths and times or the availability of day/night overlaps in satellite observations. Second, many climate and ocean modellers are reluctant to include a diurnal cycle in their models because of the increased cost of extra vertical resolution, therefore the satellite community need to provide observations for assimilation that are not contaminated by a diurnal signal. These maps can be used either to flag observations likely to have diurnal warming, or better still, the model output may be used to remove the diurnal bias. Third, this simple model approach could potentially be useful for improving accuracy in observational foundation SST products, again by removing the diurnal signal and reducing bias.

The different nature of SST observations and their model counterparts, is highlighted, as well as the lack of GCM model representations of diurnal variability. In order to reduce errors in an assimilation procedure for operational oceanography models, an observation operator is needed to transform model variables of bulk temperatures into the skin and sub-skin temperatures of satellite measured SSTs. The reverse is true for producing foundation SST observational products; for this case SST observations 'corrupted' by a diurnal signal need to be converted to the base temperature from which the diurnal thermocline has developed. A 1-D model equipped with fine near surface resolution and diurnal forcing, as developed here, could be used as an effective dynamic observation operator for the uses outlined above.

These developments in diurnal SST modelling are built on in a companion paper [33] that describes a novel data assimilation method which utilises diurnal signal information in satellite derived SST observations together with the modelled diurnal SST to further reduce uncertainties in diurnal warming estimates.

# References


[1] M. J. Bell, R. M. Forbes, and A. Hines. Assessment of the FOAM global data assimilation system for reat-time operational ocean forecasting. *J. Mar. Syst.*, 25:1–22, 2000.

[2] D. J. Bernie, S. J. Woolnough, J. M. Slingo, and E. Guilyardi. Modelling diurnal and intraseasonal variability of the ocean mixed layer. *J. Climate*, 18:1190–1202, 2005.

[3] P. Cornillon and L. Stramma. The distribution of diurnal sea surface warming events in the western Sargasso Sea. *J. Geophys. Res.*, 90:11811–11815, 1985.

[4] P. D. Craig and M. L. Banner. Modeling wave-enhanced turbulence in the ocean surface layer. *J. Phys. Oceanogr.*, 24:2546–2559, 1994.

[5] G. Danabasoglu, W. G. Large, J. J. Tribbia, P. R. Gent, and B. P. Briegleb. Diurnal coupling in the tropical oceans of CCSM3. *J. Climate*, 19:2347–2365, 2006.

[6] F. W. Dobson and S. D. Smith. Bulk models of solar radiation at sea. *Q. J. R. Meteorol. Soc.*, 114:165–182, 1988.

[7] C. J. Donlon, P. J. Minnett, C. Gentemann, T. J. Nightingale, I. J. Barton, B. Ward, and M. J. Murray. Toward improved validation of satellite sea surface temperature measurements for climate research. *J. Climate*, 15:353–369, 2002.

[8] C. J. Donlon and the GHRSST-PP Science Team. The recommended GHRSST-PP data processing specifications GDS (version 1 revision 1.5). Technical Report 17, GHRSST-PP, 2004.

[9] C. W. Fairall, E. F. Bradley, J. S. Godfrey, G. A. Wick, J. B. Edson, and G. S. Young. Cool-skin and warm-layer effects on sea surface temperature. *J. Geophys. Res.*, 101:1295–1308, 1996.

[10] C. W. Fairall, E. F. Bradley, J. E. Hare, A. A. Grachev, and J. B. Edson. Bulk parameterization of air-sea fluxes: Updates and verification for the COARE algorithm. *J. Climate*, 16:571–591, 2003.

[11] C. W. Fairall, E. F. Bradley, D. P. Rogers, J. B. Edson, and G. S. Young. Bulk parameterization of air-sea fluxes for TOGA-COARE. *J. Geophys. Res.*, 101:3747–3764, 1996.

[12] P. Flament, J. Firing, M. Sawyer, and C. Trefois. Amplitude and horizontal structure of a large sea surface warming event during the Coastal Ocean Dynamics Experiment. *J. Phys. Oceanogr.*, 24:124–139, 1994.

[13] C. Gilman and C. Garrett. Heat flux parameterization for the Mediterranean Sea: The role of atmospheric aerosols and constraints from the water budget. *J. Geophys. Res.*, 99:5119–5134, 1994.

[14] S. Hallsworth. *Modelling the diurnal variation of sea surface temperature using a one-dimensional ocean temperature model*. PhD thesis, University of Edinburgh, 2006.

[15] L. A. Horrocks, A. R. Harris, and R. W. Saunders. Modelling the diurnal thermocline for daytime bulk SST from AATSR. Technical Report FR 418, UK Met Office, 2003.

[16] N. G. Jerlov. *Marine Optics*. Elsevier, 1976.

[17] L. H. Kantha and C. A. Clayson. An improved mixed layer model for geophysical applications. *J. Geophys. Res.*, 99:25235–25266, 1994.

[18] K. B. Katsaros and A. V. Soloviev. Vanishing horizontal sea surface temperature gradients at low wind speeds. *Bound. Layer Met.*, 112:381–396, 2004.

[19] K. B. Katsaros, A. V. Soloviev, R. H. Weisberg, and M. E. Luther. Reduced horizontal sea surface temperature gradients under conditions of clear skies and weak winds. *Bound. Layer Met.*, 116:175–185, 2005.

[20] S. Kizu. Systematic errors in estimation of insolation by empirical formulas. *J. Oceanogr.*, 54:165–177, 1998.

[21] J. Kondo. Air-sea bulk transfer coefficients in diabatic conditions. *Bound. Layer Met.*, 9:91–112, 1975.

[22] E. Kraus and S. Turner. A one-dimensional model of the seasonal thermocline: The general theory and its consequences. *Tellus*, 19:98–106, 1967.

[23] W. G. Large, J. C. McWilliams, and S. C. Doney. Oceanic vertical mixing: A review and a model with a nonlocal boundary layer parameterization. *Rev. Geophys.*, 34:363–403, 1994.

[24] J. P. McCreary, K. E. Kohler, Hood R. R, S. Smith, J. Kindle, A. S. Fischer, and R. A. Weller. Influences of diurnal and intraseasonal forcing on mixed-layer and biological variability in the central Arabian Sea. *J. Geophy. Res.*, 106:7139–7155, 2001.

[25] G. L. Mellor and T. Yamada. Development of a turbulence closure model for geophysical fluid problems. *Rev. Geophys. Space Phys.*, 20:851–875, 1982.

[26] K. A. Moyer and R. A. Weller. Observations of surface forcing from the subduction experiment: A comparison with global model products and climatological datasets. *J. Climate*, 10:2725–2742, 1997.

[27] J. C. Ohlmann and D. A. Siegel. Ocean radiant heating. Part II: Parameterizing solar radiation transmission through the upper ocean. *J. Phys. Oceanogr.*, 30:1849–1865, 2000.

[28] J. C. Ohlmann, D. A. Siegel, and C. D. Mobley. Ocean radiant heating. Part I: Optical influences. *J. Phys. Oceanogr.*, 30:1833–1848, 2000.

[29] Working Group on Air-Sea Fluxes (WGASF). Intercomparison and validation of ocean-atmosphere energy flux fields, final report of the joint WCRP/SCOR working group on air-sea fluxes (SCOR working group 110). Technical report, World Climate Research Programme, 2000.

[30] C. A. Paulson and J. J. Simpson. Irradiance measurements in the upper ocean. *J. Phys. Oceanogr.*, 7:952–956, 1977.

[31] C. A. Paulson and J. J. Simpson. The temperature difference across the cool-skin of the ocean. *J. Geophys. Res.*, 86:11044–11054, 1981.

[32] S. Pimentel. *Estimation of the Diurnal Variability of Sea Surface Temperatures using Numerical Modelling and the Assimilation of Satellite Observations*. PhD thesis, University of Reading, 2007.

[33] S. Pimentel, K. Haines, and N. K. Nichols. The assimilation of satellite derived sea surface temperatures into a diurnal cycle model. University of Reading, Department of Mathematics, Numerical Analysis Report 8/2007 (submitted for publication).

[34] J. F. Price and R. A. Weller. Diurnal cycling: Observations and models of the upper ocean response to diurnal heating. *J. Geophys. Res.*, 91, 1986.

[35] R. K. Reed. On estimating insolation over the ocean. *J. Phys. Oceanogr.*, 7:482–485, 1977.

[36] R. W. Reynolds and T. M. Smith. Improved global sea surface temperature analyses using optimum inerpolation. *J. Climate*, 7:929–948, 1994.

[37] A. Rosati and K. Miyakoda. A general circulation model for upper ocean simulation. *J. Phys. Oceanogr.*, 18:1601–1626, 1988.

[38] M .E. Schiano. Insolatation over the western Mediterranean Sea: A comparison of direct measurement and Reed's formula. *J. Geophys. Res.*, 101:3831–3838, 1996.

[39] K. Shankaranarayanan and M. A. Donelan. A probabilistic approach to scatterometer function verification. *J. Geophys. Res.*, 106:19969–19990, 2001.

[40] T. Shinoda. Impact of the diurnal cycle of solar radiation on intraseasonal SST variability in the western equatorial Pacific. *J. Climate*, 18:2628–2636, 2005.

[41] T. Shinoda and H. H. Hendon. Mixed layer modeling of intraseasonal variability in the tropical western Pacific and indian oceans. *J. Climate*, 11:2668–2685, 1998.

[42] J. Stark and C. Donlon. A new high-resolution operational sea surface temperature analysis for oceanography and meteorology. *Eos Trans. AGU, Ocean Sci. Meet. Suppl.*, 87:Abstract OS12A–04, 2006.

[43] H. Stommel. Observations of the diurnal thermocline. *Deep Sea Res.*, 16:269–284, 1969.

[44] L. Stramma, P. Cornillon, R. A. Weller, J. F. Price, and M. G. Briscoe. Large diurnal sea surface temperature variability: Satellite and in situ measurements. *J. Phys. Oceanogr.*, 56:345–358, 1986.

[45] A. C. Stuart-Menteth, I. S. Robinson, and P. G. Challenor. A global study of diurnal warming using satellite-derived sea surface temperature. *J. Geophys. Res.*, 108:3155, 2003.

[46] A. C. Stuart-Menteth, I. S. Robinson, R. A. Weller, and C. J. Donlon. Sensitivity of the diurnal warm layer to meteorological fluctuations. Part 1: Observations. *Journal of Atmospheric and Ocean Science*, 10:193–208, 2005.

[47] L. Umlauf and H. Burchard. A generic length-scale equation for geophysical turbulence models. *J. Mar. Res.*, 61:235–265, 2003.

[48] L. Umlauf, H. Burchard, and K. Bolding. *General Ocean Turbulence Model. Scientific documentation. v3.2.* Marine Science Reports no. 63, Baltic Sea Research Institute Warnemnde, Warnemnde, Germany, 2005.

[49] P. J. Webster, C. A. Clayson, and J. A. Curry. Clouds, radiation, and the diurnal cycle of sea surface temperature in the tropical western Pacific. *J. Climate*, 9:1712–1730, 1996.

[50] R. A. Weller and S. P. Anderson. Surface meteorology and air-sea fluxes in the western tropical Pacific warm pool during the TOGA Coupled Ocean-Atmosphere Response Experiment. *J. Climate*, 9:1959–1990, 1996.

[51] R. A. Weller, M. F. Baumgartner, S. A. Josey, A. S. Fischer, and J. C. Kindle. Atmospheric forcing in the Arabian Sea during 1994-1995: observations and comparisons with climatology and models. *Deep-Sea Res. II*, 45:1961–1999, 1998.

[52] R. A. Weller, A. S. Fischer, D. L. Rudnick, C. C. Eriksen, T. D. Dickey, J. Marra, C. Fox, and R. Leben. Moored observations of upper-ocean response to the monsoons in the Arabian Sea during 1994-1995. *Deep-Sea Res. II*, 49:2195–2230, 2002.

[53] G. Yang and J. Slingo. The diurnal cycle in the tropics. *Mon. Wea. Rev.*, 129:784–801, 2001.